

Laser-induced fusion in ultra-dense deuterium D(-1): optimizing MeV particle emission by carrier material selection

Leif Holmlid

Atmospheric Science, Department of Chemistry and Molecular Biology, University of Gothenburg, SE-412 96 Göteborg, Sweden.
Tel.:+46317869076. E-mail address: holmlid@chem.gu.se

Abstract

Power generation by laser-induced nuclear fusion in ultra-dense deuterium D(-1) requires that the carrier material interacts correctly with D(-1) prior to the laser pulse and also during the laser pulse. In previous studies, the interaction between the superfluid D(-1) layer and various carrier materials prior to the laser pulse has been investigated. It was shown that organic polymer materials do not give a condensed D(-1) layer. Metal surfaces carry thicker D(-1) layers useful for fusion. Here, the interaction between the carrier and the nuclear fusion process is investigated by observing the MeV particle emission (e.g. 14 MeV protons) using twelve different carrier materials and two different methods of detection. Several factors have been analyzed for the performance of the carrier materials: the hardness and the melting point of the material, and the chemical properties of the surface layer. The best performance is found for the high-melting metals Ti and Ta, but also Cu performs well as carrier despite its low melting point. The unexpectedly meager performance of Ni and Ir may be due to their catalytic activity towards hydrogen which may give atomic association to deuterium molecules at the low D₂ pressure used.

Keywords: Ultra-dense deuterium, nuclear fusion, ICF, superfluid, fuel carrier, surface
PACS: 89.30.Jj, 28.52.Fa, 67.63.Gh, 68.65.k

1. Introduction

Laser-induced nuclear fusion in ultra-dense deuterium D(-1) was reported in a few recent publications [1-3]. This means that this material may be useful as a target material in laser-driven fusion. The handling of D(-1) is demanding, since D(-1) is a quantum material which is shown in experiments to be both superfluid [4] by a fountain effect [5] and probably also superconductive [6] by a Meissner effect. D(-1) gives a condensed superfluid film on metal surfaces and a decreasing surface density on adjacent organic polymer surfaces [7]. The reason for its quantum properties is the short D-D distance in the material, only 2.3 pm [8-11]. The quantum mechanical background for D(-1) was described by Winterberg [12,13]. It is apparent from this that D(-1) is similar to other superfluids in many respects. Bereziani et al. [14] predicts that a dense deuterium phase is a quantum liquid with both superfluid and superconducting properties. Different phases of this type of material have been discussed by Babaev et al. [15] and by Bedaque et al. [16]. Related results exist on a superconductive state of high density hydrogen clusters in voids (Schottky defects) measured by SQUIDS in palladium [17]. The close relation between these hydrogen clusters and D(-1) has been pointed out [18]. The interatomic distance in the hydrogen case was concluded to be close to 2 pm [19], similar to that for D(-1). The condensation effect was discussed as due to Bose-Einstein condensation [20].

The construction of laser-beam and ion-beam fusion targets with hydrogen fuel (mostly D-T mixtures) has a long history starting with the planning for inertial confinement fusion (ICF). Reports on gaseous targets exist at least from the 1980's [21]. Later, both so-called direct drive targets and indirect-drive targets [22] with the laser energy converted to high-energy photons or electrons before impact on the actual hydrogen target have been suggested and developed. The targets in these systems should both contain the fuel and help in compressing the fuel evenly under laser-beam or ion-beam impact to such a high density and temperature that fusion could take place. With the recent discovery of ultra-dense hydrogen fuels like D(-1) studied here, the problem of compressing the fuel has disappeared, since its density of 10^{29} cm⁻³ is higher than believed possible by any compression method. The problem of confinement of the fuel is almost but not completely relaxed to the problem of preventing the superfluid fuel to creep away after its formation. For ICF in D(-1) it is important both that the super-fluid properties can be controlled and that a suitable carrier material for the superfluid will exist. Thus, we here investigate the properties and intensities of the MeV particles ejected from the laser-induced fusion process in D(-1) residing on different carrier materials. It is apparent that several different types of interaction between D(-1) and the carrier surface are of concern. These may be classified as 1) interaction prior to the laser pulse, including condensation and superfluidity, 2) interaction with the laser pulse, including absorption and heating due to the laser pulse, 3) interaction during the laser pulse, including chemical interaction between the surface and deuterium, 4) interaction during the plasma expansion, including evaporation and radiation. While the previous study [7] mainly investigated the properties in phase 1 above, the present study is mainly concerned with phase 3, thus the interaction during the laser pulse.

2. Theory

Ultra-dense deuterium D(-1) has been investigated experimentally in our laboratory in a large number of published studies [1,2,8-11,23,24]. The observed kinetic energy release of up to 630 eV corresponds to a bond distance of 2.3 ± 0.1 pm in the D(-1) clusters under normal conditions [8,9]. Experiments even show a D-D distance down to 2.14 ± 0.03 pm in equilibrium at room temperature [11]. Due to the extremely high density of D(-1), of the order of 10^{29} cm⁻³ (140 kg cm⁻³) this material is believed to be very useful as target material for inertial confinement fusion (ICF) using intense pulsed lasers [8,9,25]. The best description of D(-1) so far is that it is an inverted or contracted form of the dense (metallic) form D(1). This is based on the general ideas of dense hydrogen materials by Ashcroft and other authors [26,27]. The D-D values found in the experiments are close to the theoretically expected distance for an inverted D(-1) material of $d_{-1} = (m_e/m_D)^{1/2} d_1$ equal to 2.5 pm [8]. Only hydrogen isotope atoms should give an ultra-dense material form, since the inner electrons in all other atoms will prevent the formation of such a material. A similar ultra-dense protium material called p(-1) or H(-1) also exists [28].

D(1) and D(-1) are probably the two lowest excitation levels of deuterium Rydberg Matter (RM) [29-31]. For a recent review of RM, see Ref. [32]. The energy level of D(-1) is slightly lower than that of D(1) [10]. These condensed deuterium forms are more complex than ordinary RM since they are quantum materials. The only good quantum numbers in RM in general are the orbital quantum number l and electron and nuclear spin quantum numbers. This is also the case for D(-1), where the spin quantum numbers seem to be most important. The interconversion between D(1) and D(-1) is facile and even gives an oscillation between these two forms of matter [9]. Further details of the conversion are given in Ref. [23]. The experiments show that the D(-1) clusters have the form D_{2N} , with N an integer. This shape is shown Fig. 1.

3. Experimental

The apparatus has been described in several publications, for example in [3,33]. It has a base pressure $< 1 \times 10^{-6}$ mbar. The layout of the setup used is shown in Fig. 2. The central source part has been described separately [10]. The emitter in the source is a cylindrical (extruded) sample of an industrial iron oxide catalyst doped with K (initially at 8 wt %) [34,35]. It is of the styrene catalyst type Shell S-105 which is an efficient hydrogen abstraction and transfer catalyst. The emitter is mounted in the tight-fitting opening of a metal tube which is connected to the D₂ gas feed. The source metal tube is heated by an AC current through its wall up to 400 K. Deuterium gas (> 99.8 % D₂) is admitted through the source at a pressure up to 1×10^{-5} mbar in the chamber. The D(-1) formed falls down as clusters to a plate below the source. The D(-1) phase is at a slightly lower energy level than D(1) [10], which means that it will be formed spontaneously. On the plate which is sloping at 45° angle towards the

horizontal, a foil of the surface material under test is mounted. A Nd:YAG laser with an energy of < 200 mJ per each 5 ns long pulse at 10 Hz is used at 532 nm. The laser beam is focused at the test surface with an $f = 400$ mm spherical lens. The intensity in the beam waist of (nominally) 30 μm diameter is relatively low, $\leq 4 \times 10^{12}$ W cm^{-2} as calculated for a Gaussian beam.

Two different types of experiment have been done to study the efficiency of the laser-induced fusion on various materials. One of these is here called delayed TOF (time-of-flight), and employs a scintillator-PMT (photomultiplier) detector at a distance of 112 cm from the center of the apparatus. The 5 cm thick plastic scintillator (BC-408, Saint-Gobain Crystals) has an entrance area of 20×26 mm^2 for the particle flux from the laser focus. The photomultiplier (PMT) is Electron Tubes EMI 9813B with single electron rise time of 2 ns and transit time of 46 ns. Blue glass filters in front of the PMT decrease the observed laser signal. The cathode of the PMT is covered by a light-tight Al foil and black plastic tape, leaving only 1 mm^2 open for the impinging light to decrease the very high signal. The signal is normally observed on a fast, 300 MHz digital oscilloscope with or without a fast preamplifier. Many experiments have also employed pulse counting and a fast multi-channel scaler with 5 ns time bins. Two different construction parts in the particle beam to this detector are used to block low-energy particles or delay high-energy particles as shown in Fig. 2. The inner one (closest to the target) is a box of stainless steel plate. The entrance slit to this box is at a distance of approximately 73 mm from the center. Closer to the detector, at a distance of 64 cm from the target, a beam-flag with 2-3 Al foils (each 15 μm thick) can be moved into the beam or completely out from the beam. By moving these two blocking items, the signal to the detector can be blocked or delayed, depending on the types of particles in the beam. The inner box also selects the part of the target that is observed by the detectors. When the TOF signal at the PMT detector is bimodal with two peaks of similar size, it is concluded that the second peak has been delayed either in the inner box or in the beam-flag. The energy of the initial particles in such a case is in the low MeV region.

The other type of experiment is here called fast collector measurement. It means that the signal current to the beam-flag at 64 cm from the target is measured directly with the oscilloscope with a 50 Ω coaxial input, and that the signal is analyzed (blocked or delayed) by the inner box in the apparatus. In this case, the most detailed information is found for particles with energy up to 15 MeV, in a TOF range not possible to study reliably with a PMT detector due to the long electron transport (transit) time through the PMT. To analyze the collector signal further, a shielded battery is used in the signal path to the oscilloscope to keep the collector at -24 V or +24 V. With no battery, the collector is at 0 V. With -24 V on the collector, no electrons from the plasma or due to photons from the plasma can reach the collector.

4. Results

Several different surfaces have been studied with the two methods described above. Since light atoms radiate less from a high temperature plasma, surfaces based mainly on carbon like

graphite and polymers like PTFE (polytetrafluoroethylene) and PMMA (poly(methyl methacrylate)) have been studied again [7]. For the same reason, light metal surfaces of Al and Ti have been tested. Other metal surfaces like Cu and Ni could be of interest due to their low cost. As examples of heavy, high-melting metals surfaces of Ta and Ir have been studied. The metals tested constitute a selection over the periodic table. Ti is in Group 4 and Ta in Group 5. Group 8-10 which is hydrogen active as catalysts contain the tested metals Ni and Ir. Cu belongs to Group 11 and Al to Group 13. Thus, a broad spectrum of metals is covered.

Besides plane organic polymer and metal surfaces, a few other test targets have been used. The glass-like (machinable) material Macor was studied as an example of an inorganic polymer with only relatively light atoms. The effect of a magnetic field at the carrier surface was investigated with the well-performing Ta surface. Also, a Ni foam material (Goodfellow NI003852) was tested since the foam structure gives a larger active area (95% porosity) and thus possibly more D(-1) in the laser focus. Here, the aim has only been to identify the basic carrier parameters influencing the laser-induced fusion process in D(-1) and to exclude carriers that do not function well. The results are summarized in Table 1, together with some further data for the materials tested. An example of the damage done by the fusion process on the Ta surface (melting point 3269 K) is shown in Fig. 3.

Examples of the results with the two main methods used are given in Figs. 4 and 5, both using Ti surfaces. In both cases, the maximum signal is obtained at a position of the analyzing slit 1-3° from the nominal centerline. This is due to a small displacement of the laser focus on the target in these experiments. In Fig. 4 with the fast collector results, the signal to the collector appears symmetric around +2.5° (with the analyzing slit moved 3 mm from the nominal centerline). In this measurement, both 14 MeV protons at 12 ns TOF are observed, and 5 MeV u⁻¹ particles which may be D ejected by collisions with 14 MeV protons. Such collisions give up to 6 MeV u⁻¹ on the deuterons. The well separated 14 MeV peak indicates efficient fusion $D + D \rightarrow T + p$. As soon as the slit blocks the fast particles at larger angles from the centerline, the 14 MeV peaks disappear while slower particles are still observed. This is not due to a penetration of the slower particles through the metal box, but is caused by the change in the location on the target visible to the collector when the box is moved. The 5 MeV u⁻¹ particles are thus ejected from parts outside the laser focus due to scattering of faster particles from the focus.

In Fig. 5, the signal at the PMT detector is shown in a delayed TOF measurement. The signal is given both with and without the Al foil beam-flag in the beam. Observe that the signal with flag open (to the right in the figure) has a different scale, 10 times larger. When the flag is open, the signal is largest at +3°, while with the flag closed the signal at this angle disappears almost completely. At +4°, there exists a small delayed particle signal. This indicates that the signal from the target at these positions of the analyzing slit is almost completely in particle form and thus efficiently removed by the beam-flag. This agrees with the results in Fig. 4. With the analyzing slit (steel plate) at other angles and the flag open, delayed particles are observed at 50-100 ns after the rise of the signal. This corresponds to an energy of approximately 1 MeV u⁻¹ which a proton may retain after several collisions with heavy atoms.

Thus, the protons are delayed by penetration through the steel plate, or maybe by scattering back and forth inside the steel box. At $+2^\circ$ in the figure, this signal is removed by closing the flag. At 0° the signal (which is there not delayed) is almost unchanged when the flag is closed (note the factor of 10 between the vertical scales). This indicates mainly penetrating photons from the plasma as the signal to the detector. The amount of delayed particles is used as a crude measure of the amount of MeV particles in this type of experiment.

The peak voltage of 14 MeV protons is up to 200 mV, as seen in Fig. 4. With a 50Ω input resistance in the oscilloscope, this means 4 mA of current. The viewing factor of the collector is 2×10^{-4} of the sphere, thus this current corresponds to 18 A current of 14 MeV protons assuming isotropic ejection. With this pulse lasting 5 ns, the total energy in the 14 MeV protons is 1.2 J. Thus the fusion process is close to break-even.

5. Discussion

The results are summarized in Table 1. It is seen there that the results vary strongly between different carrier materials. It is clear from earlier studies [7] that metal surfaces are preferred since organic polymer surfaces do not give a thick enough layer of D(-1) to support fusion efficiently. As seen now from the results using Macor, also inorganic polymers like this silicate based glass do not support a thick enough layer of D(-1).

Among the metals studied, a few high-melting metals like Ti and Ta are superior. These two metals also have the property that their oxides are not easily reduced by hydrogen as given in Table 1, thus their surfaces are inert and do not react easily with hydrogen. In actual use for power generation by laser-induced fusion, just a few laser pulses will be used for ignition. A surface that may give a structure that interacts deleterious with the D(-1) layer should not be used. Thus, a high-melting metal without an oxide layer or with a non-reducible oxide layer is the best choice.

In a plasma, heavy metal atoms are known to radiate strongly and cool the plasma. Thus, the optimum choice is a metal with the properties discussed above and as small atomic mass as possible, since this will give less problems in the last phase of the fusion process, called phase 4 in the Introduction. Thus, it is concluded that the best choice is Ti of the metals tested so far.

From Table 1 it is also seen that Cu behaves well as a carrier, even if it is relatively low-melting and also has a reducible oxide layer on its surface. Another interesting observation is that Ni with its higher melting point performs worse. Even more intriguing is that Ir with its high density and high melting point does not behave as well as Ti and Ta. The most likely explanation for these unexpected effects is the catalytic activity of the Ni and Ir surfaces. See for example Ref. [36] which describes the background for heterogeneous hydrogenation in catalysts. It is pointed out there that this type of activity is limited mainly to Group 8-10 metals, thus Ni and Ir in the present case. This catalytic activity means that D_2 is in (disturbed) equilibrium with 2 D atoms on the surface. If D(-1) is decomposed thermally at low density to free D atoms, D_2 may be formed and may then also desorb. If the D_2 pressure

in the chamber is high, the process will be reversed and D atoms will form on the surface, but at the low pressure used in the present experiments, it is likely that D₂ can desorb from the Ni and Ir surfaces. Thus, the performance of these surfaces as carriers of D(-1) will be decreased.

6. Conclusions

All metals tested as carriers in the laser-induced fusion of D(-1) give MeV particles, mainly protons, which are easily detected and identified by two different types of detectors in the apparatus used. For example, 14 MeV protons are measured directly as a current to a collector in time-of-flight experiments. From the amount of MeV particles for several polymers (organic and inorganic) and metals, it is concluded that a low atomic mass, high melting metal with no catalytic activity for deuterium is the best choice as fusion carrier in the present experiments. Among the tested metals, Ti is the best carrier material.

References

- [1] S. Badiei, P.U. Andersson, L. Holmlid, Laser-driven nuclear fusion D+D in ultra-dense deuterium: MeV particles formed without ignition, *Laser Part. Beams* 28 (2010) 313-317.
- [2] P.U. Andersson, L. Holmlid, Fusion generated fast particles by laser impact on ultra-dense deuterium: rapid variation with laser intensity, *J. Fusion Energ.* 31 (2012) 249-256.
- [3] L. Holmlid, MeV particles from laser-initiated processes in ultra-dense deuterium D(-1), *Eur. Phys. J. A* 48 (2012) 11.
- [4] T. Guénault, *Basic superfluids*, Taylor and Francis, London, 2003.
- [5] P.U. Andersson, L. Holmlid, Superfluid ultra-dense deuterium D(-1) at room temperature, *Phys. Lett. A* 375 (2011) 1344-1347.
- [6] P.U. Andersson, L. Holmlid, S.R. Fuelling, Search for superconductivity in ultra-dense deuterium D(-1) at room temperature: depletion of D(-1) at field strength > 0.05 T, *J. Supercond. Novel Magn.* 25 (2012) 873-882.
- [7] F. Olofson, L. Holmlid, Superfluid ultra-dense deuterium D(-1) on polymer surfaces: structure and density changes at a polymer-metal boundary, *J. Appl. Phys.* 111 (2012) 123502.
- [8] S. Badiei, P.U. Andersson, L. Holmlid, Laser-induced variable pulse-power TOF-MS and neutral time-of-flight studies of ultra-dense deuterium, *Phys. Scripta* 81 (2010) 045601.
- [9] S. Badiei, P.U. Andersson, L. Holmlid, Production of ultra-dense deuterium, a compact future fusion fuel, *Appl. Phys. Lett.* 96 (2010) 124103.
- [10] P.U. Andersson, B. Lönn, L. Holmlid, Efficient source for the production of ultra-dense deuterium D(-1) for laser-induced fusion (ICF), *Rev. Sci. Instrum.* 82 (2011) 013503.
- [11] L. Holmlid, High-charge Coulomb explosions of clusters in ultra-dense deuterium D(-1), *Int. J. Mass Spectrom.* 304 (2011) 51-56.
- [12] F. Winterberg, Ultradense Deuterium, *J. Fusion Energ.* 29 (2010) 317-321.
- [13] F. Winterberg, Ultra-dense deuterium and cold fusion claims, *Phys. Lett. A* 374 (2010) 2766-2771.
- [14] L. Berezhiani, G. Gabadadze, D. Pirtskhalava, Field Theory for a Deuteron Quantum Liquid, *J. High Energy Phys* 4 (2010) 122.
- [15] E. Babaev, A. Sudbø, N.W. Ashcroft, A superconductor to superfluid phase transition in liquid metallic hydrogen, *Nature* 431 (2004) 666-668.
- [16] P.F. Bedaque, M.I. Buchoff, A. Cherman, The phases of deuterium at extreme densities, *J. High Energy Phys* 4 (2011) 94.
- [17] A. Lipson, B.J. Heuser, C. Castano, G. Miley, B. Lyakhov, A. Mitin, Transport and magnetic anomalies below 70 K in a hydrogen-cycled Pd foil with a thermally grown oxide. *Phys. Rev. B* 72 (2005) 212507.
- [18] L. Holmlid, H. Hora, G. Miley, X. Yang, Ultrahigh-density deuterium of Rydberg matter clusters for inertial confinement fusion targets, *Laser Part. Beams* 27 (2009) 529-532.
- [19] H. Hora, G.H. Miley, Maruhn-Greiner maximum of uranium fission for confirmation of low energy nuclear reactions LENR via a compound nucleus with double magic numbers. *J. Fusion Energ.* 26, 349-355.

- [20] G.H. Miley, H. Hora, K. Philberth, A. Lipson, P.L. Shrestha, Radiochemical comparisons on low energy nuclear reactions and uranium. In *Low-Energy Nuclear Reactions and New Energy Technologies Source Book* (Jan Marwan and Steven B. Krivit, Eds.), Vol. 2, p. 235-252. Washington, DC: American Chemical Society/Oxford University Press.
- [21] R. Mah, D.V. Duchane, A.T. Young, R.L. Rhorer, Target fabrication for inertial confinement fusion research, *Nucl. Instrum Meth. B* 10/11 (1985) 473-477.
- [22] N.A. Tahir, D.H.H. Hoffmann, J.A. Maruhn, C. Deutsch, Indirect drive inertial fusion using heavy ion cluster beams, *Nucl. Instrum Meth. B* 88 (1994) 127-130.
- [23] L. Holmlid, Deuterium clusters D_N and mixed K-D and D-H clusters of Rydberg Matter: high temperatures and strong coupling to ultra-dense deuterium, *J. Clust. Sci.* 23 (2012) 95-114.
- [24] P.U. Andersson, L. Holmlid, Cluster ions D_N^+ ejected from dense and ultra-dense deuterium by Coulomb explosions: fragment rotation and D^+ backscattering from ultra-dense clusters in the surface phase, *Int. J. Mass Spectrom.* 310 (2012) 32-43.
- [25] P.U. Andersson, L. Holmlid, Ultra-dense deuterium: a possible nuclear fuel for inertial confinement fusion (ICF), *Phys. Lett. A* 373 (2009) 3067-3070.
- [26] N.W. Ashcroft, Metallic superfluids, *J. Low Temp. Phys.* 139 (2005) 711-726.
- [27] B. Militzer, R.L. Graham, Simulations of dense atomic hydrogen in the Wigner crystal phase, *J. Phys. Chem. Solids* 67 (2006) 2136-2143.
- [28] F. Olofson, L. Holmlid, Detection of MeV particles from ultra-dense protium p(-1): laser-initiated self-compression from p(1), *Nucl. Instr. Meth. B* 278 (2012) 34-41.
- [29] E.A. Manykin, M.I. Ojovan, P.P. Poluektov, Rydberg matter: properties and decay, *Proc. SPIE* 6181 (2006) 618105-1-9.
- [30] É.A. Manykin, M.I. Ozhovan, P.P. Poluéktov, Condensed states of excited cesium atoms, *Sov. Phys. JETP* 75 (1992) 440-445.
- [31] L. Holmlid, Classical energy calculations with electron correlation of condensed excited states - Rydberg Matter, *Chem. Phys.* 237 (1998) 11-19.
- [32] L. Holmlid, Experimental studies and observations of clusters of Rydberg matter and its extreme forms, *J. Cluster Sci.* 23 (2012) 5-34.
- [33] S. Badiei, L. Holmlid, Experimental studies of fast fragments of H Rydberg matter, *J. Phys. B: At. Mol. Opt. Phys.* 39 (2006) 4191-4212.
- [34] G.R. Meima, P.G. Menon, Catalyst deactivation phenomena in styrene production, *Appl. Catal. A* 212 (2001) 239-245.
- [35] M. Muhler, R. Schlögl, G. Ertl, The nature of the iron oxide-based catalyst for dehydrogenation of ethylbenzene to styrene. 2. Surface chemistry of the active phase, *J. Catal.* 138 (1992) 413-444.
- [36] P. Gallezot, Hydrogenation – Heterogeneous, in *Encyclopedia of Catalysis*, John Wiley and Sons, Inc., 2002, DOI: 10.1002/0471227617.eoc114, sect. 3.1.
- [37] *Handbook of Chemistry and Physics, Electrochemical Series*, P. Vanýsek Ed., 92nd ed, 2011-2012, CRC.

Table 1. Experimental results for and selected properties of the used carrier materials for D+D fusion in D(-1), in order of increasing atomic mass. Bulk modulus is from open sources, including manufacturer's data sheets. The status of the oxide is determined from various data. The E values given [37] correspond to processes of the type $\text{NiO}_2 + 4 \text{H}^+ + 2\text{e}^- \rightleftharpoons \text{Ni}^{2+} + 2\text{H}_2\text{O}$.

Carrier	D(-1) layer	Fast collector signal	Delayed TOF signal	Performance as carrier	Melting temp. (K)	Reducible surface oxide; E (V)	Bulk modulus (GPa)	Typical atom mass (au)
Graphite	No	Low	Yes	Low	3900	No oxide	33	12
PMMA	No	Low	No	Low	< 360	--	≈ 2	12, 16
PTFE	Fracti on	Low	No	Low	< 530	--	< 1	12, 19
Al	Yes	Medium	No	Low	933	No	75	27
Macor	Fracti on	Not tested	--	Low	<1300	Yes (Si) 0.857	(67)	28, 39
Ti	Yes	High	Yes	High	1948	No -0.502	108	48
Stainless steel (aust.)	Yes	Medium	Yes	Medium	<1720	Yes (Fe) 0.16	≈ 200	56, 59
Ni	Yes	Medium	No	Medium	1726	Yes 1.68	177	59
Ni foam	Yes	Not tested	No	Low		Yes 1.68		1, 59
Cu	Yes	High	Yes	High	1356	Yes 2.0	140	64
Ta	Yes	High	Yes	High	3269	No -0.750	196	181
Ta (<i>B</i> field)	Yes	High	Yes	High	3269	No -0.750	196	181
Ir	Yes	High	Small	Medium - high	2680	No oxide 0.098	370	192

Figure captions

Fig. 1. Shape of the chain or “bead” clusters D_{2N} forming the superfluid phase D(-1). Each pair D_2 revolves around their common center of mass where the electrons also are centered.

Fig. 2. Schematic horizontal cut of the apparatus, showing the details of the scintillator-PMT detector.

Fig. 3. Ta foil ($10 \times 20 \text{ mm}^2$) after laser ignition of fusion in D(-1) on its surface. The laser beam has been moved vertically and horizontally, giving clear central marks as well as broader marks of the plasma region, with a width of up to 2 mm. The melting point of Ta is 3269 K and the power in the laser beam was 1 W. The hole and heat influenced region to the lower left is due to a similar previous experiment on the back side of the 0.25 mm thick foil.

Fig. 4. The collector signal with 0 V on the collector with a Ti target. The variation with the inner plate box position is shown. The signal at 14 MeV u^{-1} agrees with protons from the fusion process, while the broad bump centered at 5 MeV u^{-1} may be due to several processes like D ejected by collisions with protons, and 3 MeV protons from the fusion.

Fig. 5. Results from a delayed time-of-flight experiment using the PMT detector in Fig. 2 and a Ti carrier. Signal with and without the Al-foil beam-flag in the particle flux to the detector is shown. Note the different vertical scales, a factor of 10 higher with the beam-flag open, to the right. As in Fig. 4, the position (in degrees) for the analyzing inner slit is shown relative to the design center position. Stars * indicate delayed particles. At 0° , the signal is almost unchanged by the beam-flag indicating penetrating photons, while at $+4^\circ$, the signal is removed completely by the beam-flag, indicating massive particles (protons).

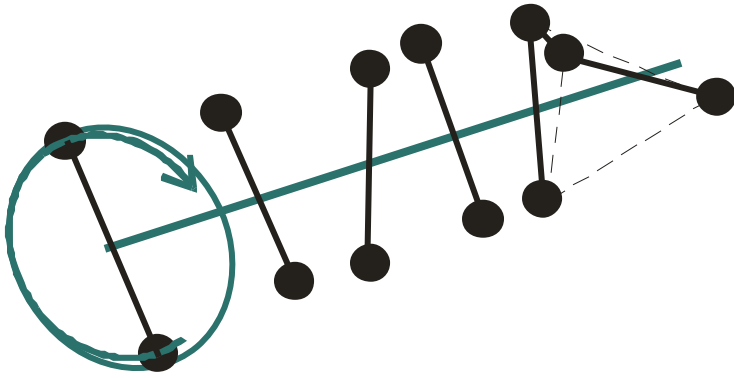


Fig. 1

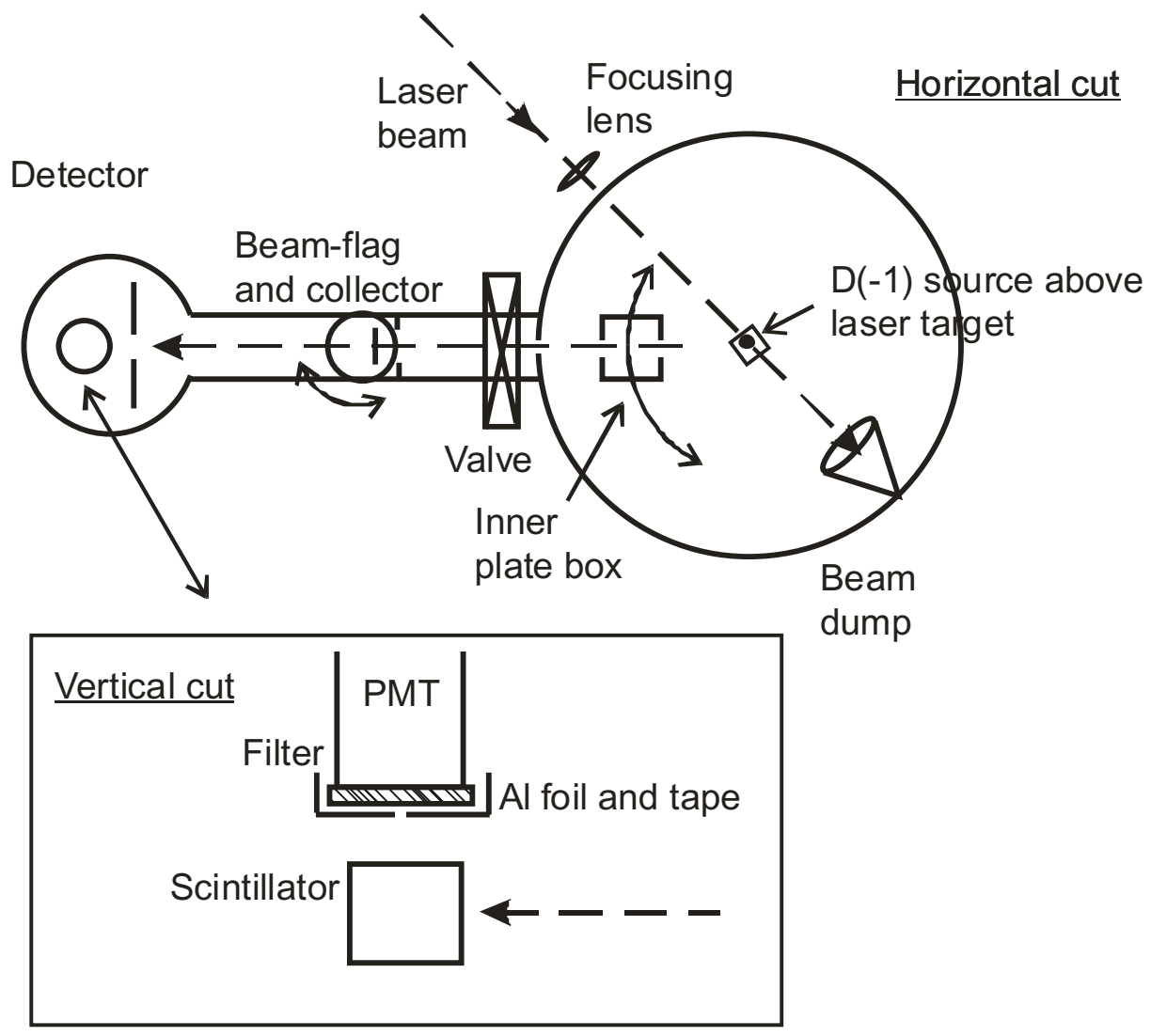


Fig. 2



Fig. 3

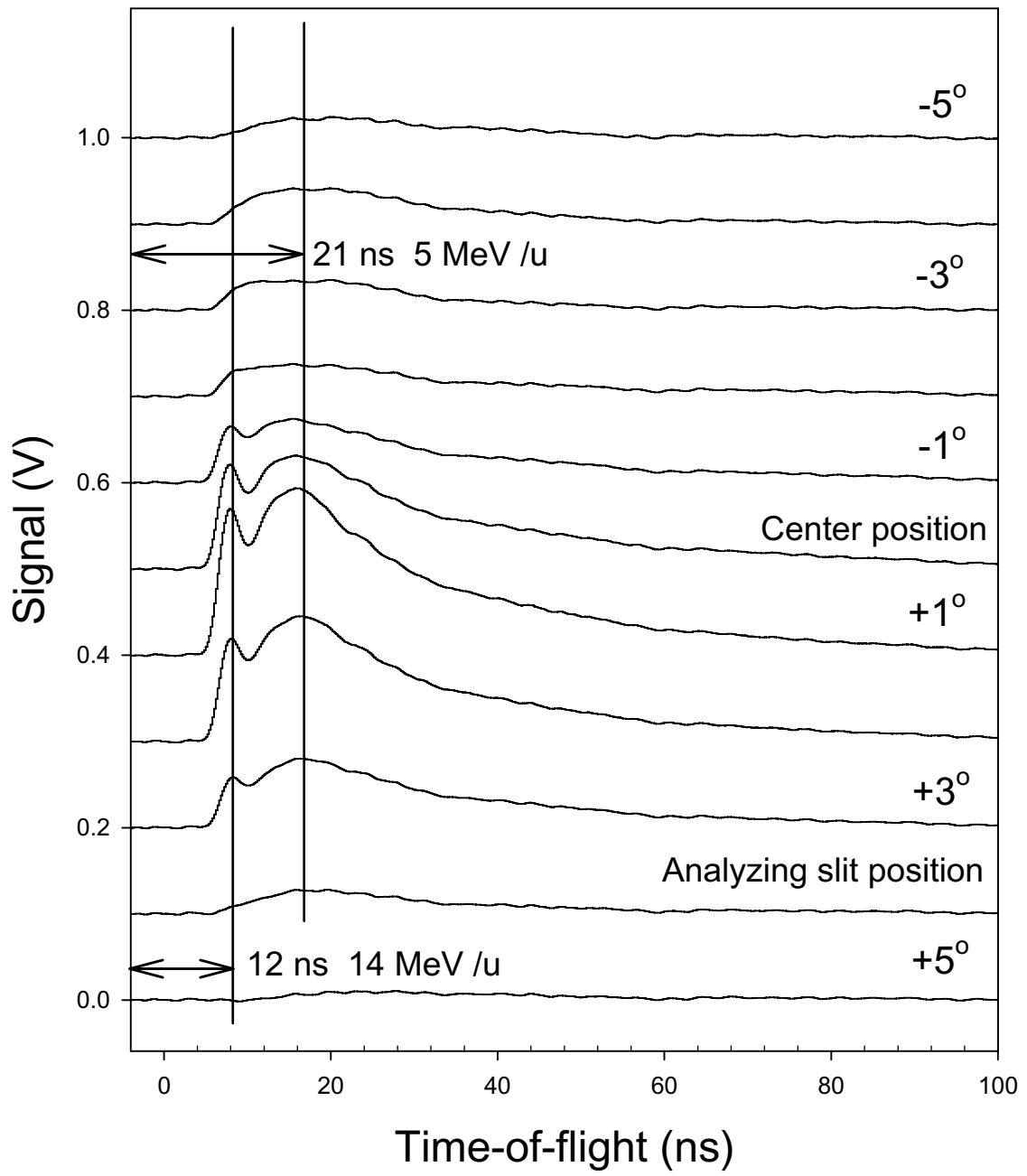


Fig. 4

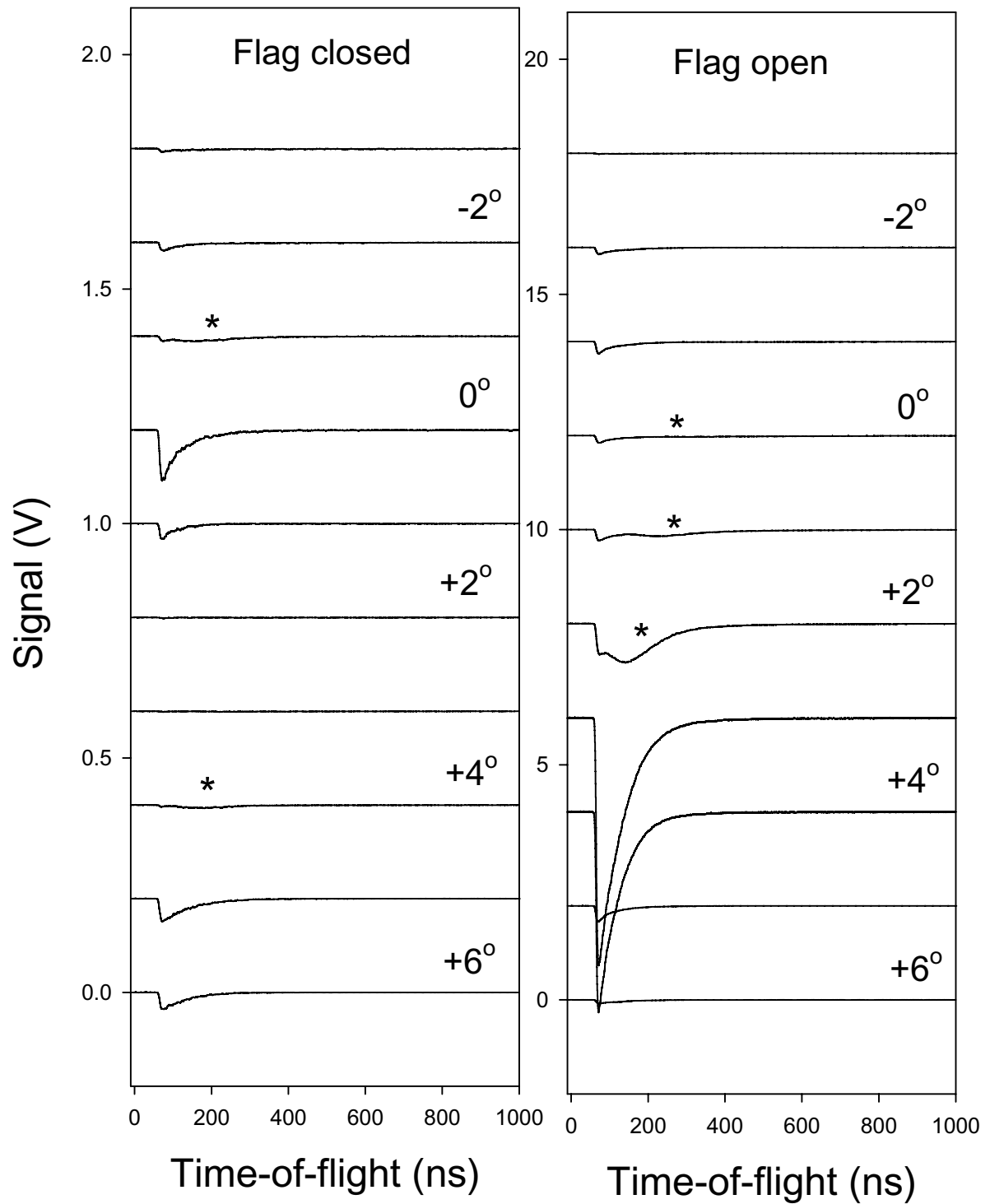


Fig. 5